Appl. Phys. B (2016) 122:105
DOI 10.1007/s00340-016-6384-1

Applied Physics B
Lasers and Optics

# Passive Q-switching of Yb bulk lasers by a graphene saturable absorber

P. A. Loiko[1,2] · J. M. Serres[1] · X. Mateos[1,3] · J. Liu[4] · H. Zhang[5] · A. S. Yasukevich[2] · K. V. Yumashev[2] · V. Petrov[3] · U. Griebner[3] · M. Aguiló[1] · F. Díaz[1]

Received: 20 December 2015 / Accepted: 9 March 2016 / Published online: 13 April 2016


**Abstract** Compact Yb:KLu$(WO_4)_2$ and Yb:$LuVO_4$ lasers diode-pumped at 978 nm are passively Q-switched by a single-layer graphene saturable absorber. The Yb:KLu$(WO_4)_2$ laser generated 165 ns/0.49 μJ pulses at 1030 nm with 170 mW average output power and 12 % slope efficiency. With the Yb:$LuVO_4$ laser, 152 ns/0.83 μJ pulses were achieved. The output power reached 300 mW at 1024 nm, and the slope efficiency was 10 %. Laser operation in a plano-plano cavity is achieved with both crystals with thermal lensing playing a key role in their performance. A model describing graphene Q-switched Yb lasers is developed. Our results indicate the potential of graphene for passive Q-switching of ~1 μm bulk lasers.

✉ X. Mateos
xavier.mateos@urv.cat; mateos@mbi-berlin.de

1 Física i Cristal·lografia de Materials i Nanomaterials (FiCMA-FiCNA), Universitat Rovira i Virgili (URV), Campus Sescelades, c/Marcel·lí Domingo, s/n., 43007 Tarragona, Spain

2 Center for Optical Materials and Technologies, Belarusian National Technical University, 65/17 Nezavisimosti Ave., 220013 Minsk, Belarus

3 Max Born Institute for Nonlinear Optics and Short Pulse Spectroscopy, 2A Max-Born-Str., 12489 Berlin, Germany

4 College of Physics, Qingdao University, 308 Ning-Xia Road, Qingdao 266071, China

5 State Key Laboratory of Crystal Materials and Institute of Crystal Materials, Shandong University, Jinan 250100, China

## 1 Introduction

The ytterbium ion ($Yb^{3+}$) is attractive for laser operation near 1 μm ($^2F_{5/2} \rightarrow {}^2F_{7/2}$ transition). Yb lasers can be pumped with commercial high-power InGaAs laser diodes emitting at 930–980 nm. The simple energy level scheme of the $Yb^{3+}$ ion and the associated absence of parasitic processes like up-conversion and excited-state absorption lead to a low heat loading and exceptionally high slope efficiencies (>80 %). In addition, some tuning of the laser wavelength is also possible with Yb lasers, similar to vibronic transition metal lasers.

In recent years, two crystal families attracted attention for $Yb^{3+}$ doping; these are the monoclinic double tungstates, KRE$(WO_4)_2$ [1], and tetragonal vanadates, $REVO_4$ [2, 3] (where RE stands for a "passive" element like Gd, Y or Lu). Both crystal families offer attractive spectroscopic properties [1, 2], in particular highest absorption and stimulated-emission cross sections (among the known hosts for $Yb^{3+}$ ions) with a strong polarization anisotropy and relatively broad emission bands. $REVO_4$ crystals are characterized with good thermal [4] and thermo-optical properties [5] that can compete with YAG. The feature of KRE$(WO_4)_2$ host is the large dopant ion–ion separation which enables doping with $Yb^{3+}$ ions at very high concentrations [6] that enables engineering of various geometries of the active medium [7, 8]. Among "passive" $RE^{3+}$ ions, lutetium ($Lu^{3+}$) is the most suitable one to be substituted by $Yb^{3+}$ due to a close matching of their ionic radii. Indeed, for an eightfold oxygen coordination, $R(Lu^{3+}) = 0.977$ Å and $R(Yb^{3+}) = 0.985$ Å. This closeness of ionic radii implies low distortions of the crystalline lattice and good optical quality. Thus, Yb:KLu$(WO_4)_2$ and Yb:$LuVO_4$ crystals are very promising for the development of efficient and high reliable Yb lasers.

Efficient Yb:KLu$(WO_4)_2$ and Yb:$LuVO_4$ lasers working in the continuous-wave (CW) [9, 10], Q-switched [11] and mode-locked [12, 13] operation modes were reported previously. In particular, passive Q-switching (PQS) of a solid-state laser with a saturable absorber (SA) is a commonly used method to produce nanosecond-long pulses from a compact and reliable all-solid device that does not require external control like for the active Q-switching. Recently, novel types of SAs based on carbon nanostructures (e.g., graphene and carbon nanotubes) emerged as suitable absorbers for PQS.

Graphene is a two-dimensional material composed of a single layer of carbon atoms arranged in a honeycomb lattice. It shows relatively strong linear absorption (2.3 % for a single layer) with a weak wavelength dependence [14] as well as absorption saturation, that is, of practical use for PQS and mode locking [15]. Graphene-SAs exhibit a high damage threshold, low saturation intensity and ultrafast carrier dynamics [16, 17]. To date, graphene-SAs have been used for PQS of Yb lasers basically in the waveguide [18–20] and fiber [21–23] configurations. Although generation of sub-100 ns pulses was demonstrated, pulse energies remained relatively low (typically, tens of nJ).

In the present paper, we aimed to realize compact Yb:KLu$(WO_4)_2$ and Yb:$LuVO_4$ lasers passively Q-switched with a graphene-SA. Graphene PQS of bulk Yb lasers can provide significant improvement in the pulse energy, while the use of compact cavity design (including plano-plano one) is beneficial for the reduction in the pulse duration. In addition, using graphene high pulse repetition frequencies are possible up to the MHz level.

## 2 Experimental

Two laser crystals were studied, namely Yb:KLu$(WO_4)_2$ (or Yb:KLuW) and Yb:$LuVO_4$. The Yb:KLuW crystal was grown by the top-seeded solution growth slow-cooling (TSSG-SC) method using a *b*-oriented seed. It was 3 at.% Yb doped (the actual ion density $N_{Yb}$ measured with electron probe microanalysis, EPMA, was $1.80 \times 10^{-20}$ at/cm$^3$). The active element from this crystal was cut along the $N_g$ optical indicatrix axis and it was 1.5 mm thick. Both $3 \times 3$ mm$^2$ $m \times p$ faces of the element were polished to laser quality and remained uncoated. The Yb:$LuVO_4$ crystal was grown by the conventional Czochralski method along the *a*-axis. It was 1.5 at.% Yb doped ($N_{Yb} = 2.04 \times 10^{-20}$ at/cm$^3$). The 2.0-mm-thick active element was *a*-cut and its faces, $3.3(c) \times 3.3$ mm$^2$, were polished but remained uncoated. The active elements were mounted in a copper holder water-cooled to 12 °C using indium foil to improve the thermal contact. The parameters of the studied laser crystals are summarized in Table 1.

**Table 1** Parameters of the studied Yb:KLuW and Yb:$LuVO_4$ crystals

| Parameter | Yb:KLuW | Yb:$LuVO_4$ |
|---|---|---|
| Growth method | TSSG | Czochralski |
| Crystal class | Monoclinic/biaxial | Tetragonal/uniaxial |
| Yb doping | 3.0 at.% | 1.5 at.% |
| $N_{Yb}$ ($10^{-20}$ at/cm$^3$) | 1.80 | 2.04 |
| Crystal cut | $N_g$-cut | *a*-cut |
| Aperture (mm$^2$) | $3.0(m) \times 3.0(p)$ | $3.3(c) \times 3.3$ |
| Thickness (mm) | 1.5 | 2.0 |

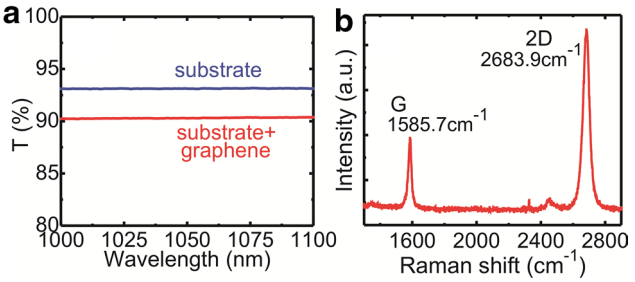


**Fig. 1** Characterization of the graphene-SA: **a** transmission spectrum, $T$(substrate + graphene)/$T$(substrate) = 97.8 %. **b** Raman spectrum

The chosen Yb doping levels are typical for KLuW and $LuVO_4$ host crystals. In the particular case of Yb:$LuVO_4$, low doping is required to maintain a good crystal quality. For both materials, the chosen doping ensured uniform heat distribution under diode pumping and prevented their stress fracture.

The laser cavity consisted of a flat pump mirror (PM) antireflection (AR) coated for 0.9–1.0 μm and high-reflection (HR) coated for 1.02–1.20 μm and a flat or concave ($R$ = 50 mm) output coupler (OC) with transmission, $T_{OC}$ = 5 or 10 % at the laser wavelength. A commercial transmission-type graphene saturable absorber (SA) from Graphene Supermarket was inserted at normal incidence between the crystal and the OC. The SA consisted of a 1.05-mm-thick fused silica substrate with a single-layer graphene deposited by the chemical vapor deposition (CVD) method. The clean face of the substrate was uncoated. The initial transmission of the graphene-SA at the laser wavelength, $T$ (substrate + graphene)/$T$ (substrate) = 97.8 %, Fig. 1a. This agrees well with the universal transmission of a single-layer graphene, $T = 1 - \pi\alpha \approx 97.7$ % ($\alpha$ is the fine structure constant). The characterization of this sample with Raman spectroscopy indicates a ratio of the integrated areas of the 2D and G bands of ~4, confirming the presence of a single carbon layer [24], Fig. 1b. The air gaps between PM, laser crystal, SA and OC were all below 0.5 mm, thus resulting in a total geometrical cavity length of ~4 mm.

The cavity configuration with the flat or concave OC will be called plano-plano or plano-concave, respectively. The laser operating with the plano-plano cavity represented the first step to the true microchip setup. In this case, all cavity elements were placed in contact with each other without air gaps.

The laser crystal was pumped by a fiber-coupled (fiber core diameter: 200 μm, N.A.: 0.22) InGaAs laser diode at ~978 nm. The lens assembly with imaging ratio 1:1 provided a pump spot radius in the crystal of $w_p = 100$ μm; the confocal parameter $2z_R$ was 3.2 mm. The total absorption in the crystal amounted to 29 % for Yb:KLuW and 51 % for Yb:$LuVO_4$. No bleaching of the crystal absorption was observed under unpolarized pumping. A fast (200 ps) InGaAs photodiode and 2 GHz Tektronix DPO5204B digital oscilloscope were used for detection of the Q-switched pulses.

## 3 Results and discussion

First, let us discuss the choice of the laser cavity geometry for Q-switching experiments. Although graphene shows almost wavelength-insensitive linear absorption from ~0.5 μm up to at least ~3 μm (~2.3 %), its nonlinear properties show strong dispersion. In particular, the saturation intensity $I_{sat}$ increases with the photon energy $h\nu$ and, as a result, $I_{sat}$ (1 μm) is almost twice higher than $I_{sat}$ (2 μm) [16]. Thus, deep saturation of graphene-SA in Yb laser requires special efforts by providing high intracavity intensity which can be reached by the reduction in the size of the laser mode on the SA. Second, due to very low saturable absorption (~0.1 %), the typical pulse durations in graphene Q-switched lasers are from few hundreds of nanoseconds to few microseconds. The improvement in this parameter requires a reduction in the cavity roundtrip time. Compact plano-concave and plano-plano cavities can provide the generation of ns Q-switched pulses, as well as small size of the laser mode on the SA.

The input–output dependences for the PQS regime of the Yb:KLuW and Yb:$LuVO_4$ lasers are presented in Fig. 2a. The laser emission was linearly polarized, $E \| N_m$. For the plano-concave cavity, stable PQS was achieved with both OCs. For $T_{OC} = 10$ %, the maximum average output power of 170 mW was achieved with a slope efficiency $\eta = 12$ % (with respect to the absorbed pump power, $P_{abs}$). The laser threshold was at $P_{abs} = 1.6$ W and the Q-switching conversion efficiency with respect to the CW mode $\eta_{conv}$ (when the SA was removed from the cavity) amounted to 22 %. For 5 % OC, the laser performance was deteriorated. The maximum output power only reached 81 mW and $\eta = 7$ %. In the plano-plano cavity configuration, stable PQS was achieved only for $T_{OC} = 10$ %. The maximum output power

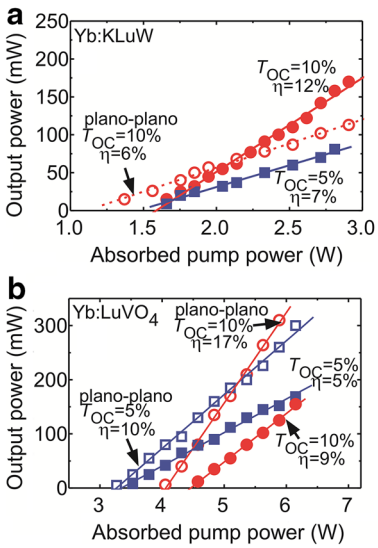


**Fig. 2** Input–output dependences of the graphene-SA passively Q-switched lasers: **a** Yb:KLuW and **b** Yb:$LuVO_4$: *open symbols*—plano-plano cavity, *filled symbols*—plano-concave cavity, *lines* are the fitting of the experimental data for the slope ($\eta$) calculation

was 113 mW and the slope efficiency was $\eta = 6$ %, that is, lower than for the plano-concave cavity; however, the laser threshold was reduced to $P_{abs} = 1.2$ W.

For the Yb:$LuVO_4$ laser, stable PQS was achieved for all the studied cavity configurations, as shown in Fig. 2b. The emission from this laser was linearly polarized, $E \| c$ ($\pi$-polarized) which agrees with previous results with *a*-cut Yb:$LuVO_4$ active elements [10]. The best results in terms of the output power (310 mW) and slope efficiency (17 %) corresponded to the plano-plano cavity and $T_{OC} = 10$ %. The Q-switching conversion efficiency was 37 %. The laser threshold, however, was at ~4.0 W which is attributed to the inferior crystal quality (as compared with Yb:KLuW). For 5 % OC, a similar level of output power was achieved (300 mW) with a reduced $\eta = 10$ %. For the plano-concave cavity, the results were inferior. Indeed, for $T_{OC} = 10$ or 5 %, the Yb:$LuVO_4$ laser generated only 155 mW with $\eta = 9$ % or 169 mW with $\eta = 5$ %, respectively. Modeling of the performance of Yb:KLuW and Yb:$LuVO_4$ lasers yielded ~4 % round-trip loss for the graphene-SA that limited the Q-switching conversion efficiency, in addition to the loss related to the Fresnel reflection from an uncoated substrate. As it will be shown later, this corresponded to non-saturable loss in the graphene-SA.

For both Yb:KLuW and Yb:$LuVO_4$ lasers, an upper limit for stable PQS existed: The laser cavity was still stable and no drop of the output power was observed; however, it was difficult to achieve a stable train of Q-switched pulses. It was observed at $P_{abs}$ ~ 3 W for Yb:KLuW laser and ~6.2 W for Yb:$LuVO_4$. It corresponded to the same level of residual

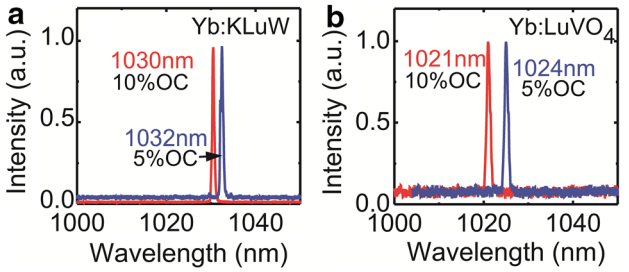


**Fig. 3** Emission spectra of the graphene-SA passively Q-switched lasers: **a** Yb:KLuW ($P_{abs}$ = 2.9 W), and **b** Yb:$LuVO_4$ ($P_{abs}$ = 6.1 W, plano-concave cavity)

(non-absorbed) pump power, ~5 W. Intensity instabilities in graphene Q-switched compact lasers are attributed to the heating of the SA due to the residual pump [25]. A mismatch of the thermal expansion coefficients for graphene and substrate (fused silica) [26] causes a compressive strain in the graphene layer with rising temperature and can, in principle, lead to its slip or buckling from the substrate surface. This can lead to a spatially nonuniform increase in the non-saturable losses in graphene-SA. However, no damage of the graphene-SA was observed in our experiments.

The emission spectra from the Yb:KLuW and Yb:$LuVO_4$ lasers are shown in Fig. 3. For both lasers, the spectra consisted of a single narrow (full width at half maximum, FWHM < 0.5 nm) emission line that was centered at 1030 or 1032 nm for Yb:KLuW and 1021 or 1024 nm for Yb:$LuVO_4$ (for $T_{OC}$ = 5 or 10 %, respectively). The observed blue shift of the emission wavelength with the increase in output coupling is typical for quasi-three-level Yb lasers and it is in accordance with the gain spectra [1]. The spectra were clearly different from those in CW regime where a multi-peak behavior was observed.

For Yb:KLuW, the shortest Q-switched pulses were obtained with the plano-concave cavity and $T_{OC}$ = 10 %. The corresponding dependence of the pulse duration (FWHM) and pulse repetition frequency (PRF) is shown in Fig. 4a. With the increase in pump level from 1.6 to 2.9 W of absorbed power, the pulse duration shortened from ~800 to 165 ns (this dependence shows a saturation for $P_{abs}$ > 2.5 W) and the PRF increased nearly linearly from 60 to 350 kHz. The saturation of the pulse duration dependence is attributed to the nearly complete saturation of the graphene-SA. The use of 5 % OC provided slightly longer pulses, 210 ns at PRF = 320 kHz. For the Yb:KLuW laser with the plano-plano cavity (using $T_{OC}$ = 10 %), 280 ns pulses were achieved at a PRF of 240 kHz. For the Yb:$LuVO_4$ laser, the shortest Q-switched pulses (152 ns, PRF = 360 kHz) were generated using the plano-plano cavity configuration and $T_{OC}$ = 5 %, as shown in Fig. 4b. Similar pulse characteristics (165 ns/340 kHz) were

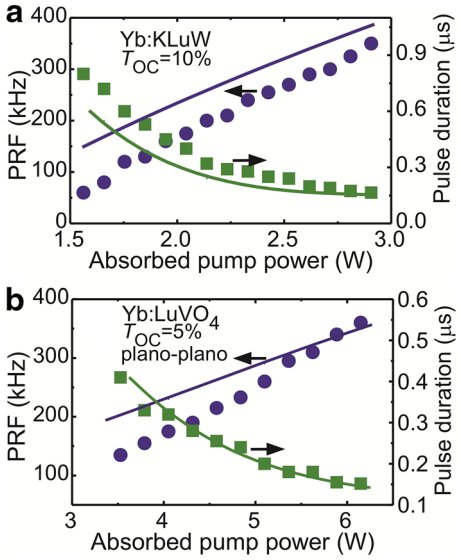


**Fig. 4** Pulse duration (FWHM) and pulse repetition frequency (PRF) of the graphene-SA passively Q-switched **a** Yb:KLuW laser ($T_{OC}$ = 10 %), **b** Yb:$LuVO_4$ laser with the plano-plano cavity ($T_{OC}$ = 5 %); *symbols* are the experimental data; *curves* refer to the modeling

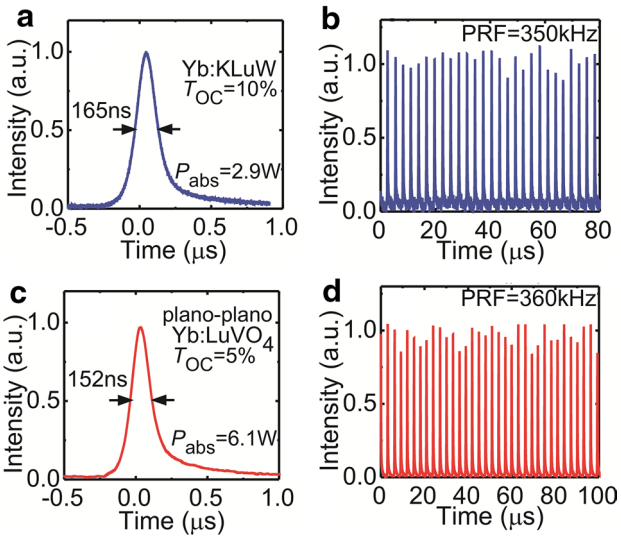


**Fig. 5** Single pulse and pulse train records for graphene-SA passively Q-switched **a**, **b** Yb:KLuW laser with the plano-concave cavity ($T_{OC}$ = 10 %) and **c**, **d** Yb:$LuVO_4$ laser with the plano-plano cavity ($T_{OC}$ = 5 %)

detected for this OC using the plano-concave cavity. For 10 % OC, much longer pulses were achieved.

The oscilloscope records of the shortest Q-switched pulses and the corresponding pulse trains obtained for Yb:KLuW and Yb:$LuVO_4$ lasers are shown in Fig. 5. The intensity instabilities in the pulse trains were ~15 %. This value is determined by the above-mentioned heating of

graphene-SA. An asymmetric shape of the single pulses indicates that the ratio between the initial transmission of the graphene-SA (that can be varied by the number of graphene layers $n$) and the output coupler transmission can be further optimized.

By using the data on the average output power, PRF and pulse duration, we calculated the pulse energies ($E_{out} = P_{out}$/PRF) and peak powers ($P_{peak} = E_{out}/\tau$) for the Yb:KLuW and Yb: $LuVO_4$ lasers. For the Yb:KLuW laser with a plano-concave cavity, the maximum pulse energy reached 0.49 μJ and it corresponded to a maximum peak power of 3.0 W ($T_{OC} = 10$ %). Yb:$LuVO_4$ laser with the plano-plano cavity provided a nearly twofold increase in the two parameters, 0.94 μJ/3.9 W and 0.84 μJ/5.5 W for $T_{OC} = 10$ and 5 %, respectively. The pulse energy and peak power dependences on the absorbed pump power for the described lasers are presented in Fig. 6. The peak power increased nearly linear with $P_{abs}$, while the pulse energy was saturated at high pump levels, probably due to the heating of the SA.

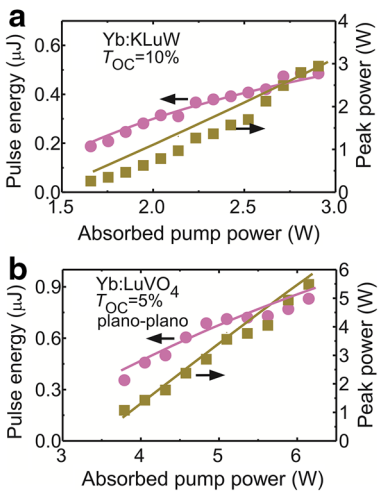


**Fig. 6** Pulse energy and peak power of the graphene-SA passively Q-switched **a** Yb:KLuW laser with the plano-concave cavity ($T_{OC} = 10$ %), **b** Yb:$LuVO_4$ laser with the plano-plano cavity ($T_{OC} = 5$ %): *symbols* are the experimental data, *curves* refer to the modeling

A summary of the PQS performance of Yb:KLuW and Yb:$LuVO_4$ lasers is presented in Table 2.

The different behavior of Yb:KLuW and Yb:$LuVO_4$ lasers for plano-concave and plano-plano cavity configurations can be explained considering the intracavity peak intensity on the SA, $I_{in}$. In order to calculate $I_{in}$, we considered the spatial and temporal distribution of the laser beam. In the assumption of $TEM_{00}$ laser mode and nearly Gaussian temporal profile of single pulses, $I_{in} = X[2E_{out}/\pi w_l^2\tau^*]$, where $X = (1 + R)/(1 - R)$ and $R$ is the reflectivity of the OC, $w_l$ is the radius of the laser mode, the term "2" indicates Gaussian spatial profile and $\tau^* \approx 1.06\tau$ is the effective pulse duration. To estimate the value of the laser waist ($w_l$), first we calculated the sensitivity factor of the thermal lens [27], $M = 2.1$ and 3.7 $m^{-1}$/W for Yb:KLuW and Yb:$LuVO_4$ crystals, respectively. Thus, the value of $w_l$ for the plano-plano/plano-concave cavities was ~61/42 μm (for Yb:KLuW) and ~44/38 μm (for Yb:$LuVO_4$), respectively, that was always below the radius of the pump beam, $w_p$. The results on $I_{in}$ are then summarized in Table 3. The values $I_{in}$ should be compared with the typical value of saturation intensity for CVD-grown single-layer graphene, $I_{sat}$ ~ 0.7–1 MW/$cm^2$ at ~1 μm [16].

For the Yb:KLuW laser with a weaker thermal lens than Yb:$LuVO_4$, the use of concave OC has a significant effect on the laser mode and, hence, on the intracavity intensity. For Yb:KLuW laser with the plano-plano cavity, $I_{in}$ ~ 0.6 MW/$cm^2$ that is slightly below the $I_{sat}$ value. However, for the plano-concave cavity, $I_{in}$ is ~2 times higher than the saturation intensity. This means stronger bleaching of the SA and, consequently, generation of shorter pulses, as given in Table 2. For the Yb:$LuVO_4$ laser with a stronger

**Table 2** Output characteristics of the Yb:KLuW and Yb:$LuVO_4$ lasers passively Q-switched with a single-layer graphene-SA

| Cavity | $T_{OC}$ (%) | $P_{th}$ (W) | $P_{out}$ (mW) | $\eta$ (%) | $\eta_{conv}$ (%) | $\tau$ (ns) | PRF (kHz) | $E_{out}$ (μJ) | $P_{peak}$ (W) |
|---|---|---|---|---|---|---|---|---|---|
| Yb:KLuW | | | | | | | | | |
| Plano-concave | 10 | 1.6 | 170 | 12 | 22 | 165 | 350 | 0.49 | 3.0 |
| | 5 | 1.5 | 81 | 7 | 7 | 210 | 320 | 0.25 | 1.2 |
| Plano-plano | 10 | 1.2 | 113 | 6 | 13 | 280 | 240 | 0.47 | 1.7 |
| | 5 | Unstable PQS | | | | | | | |
| Yb:$LuVO_4$ | | | | | | | | | |
| Plano-concave | 10 | 4.6 | 155 | 9 | 35 | 190 | 270 | 0.57 | 3.0 |
| | 5 | 3.5 | 169 | 5 | 19 | 165 | 340 | 0.50 | 3.0 |
| Plano-plano | 10 | 4.0 | 310 | 17 | 37 | 240 | 330 | 0.94 | 3.9 |
| | 5 | 3.2 | 300 | 10 | 28 | 152 | 360 | 0.83 | 5.5 |

$P_{th}$, laser threshold; $P_{out}$, output power; $\eta$, slope efficiency; $\eta_{conv}$, Q-switching conversion efficiency; $\tau$, pulse duration; PRF, pulse repetition frequency; $E_{out}$, pulse energy; $P_{peak}$, peak power

**Table 3** Mode-matching analysis and intracavity peak intensity for graphene Q-switched Yb:KLuW and Yb:$LuVO_4$ lasers

| Crystal | $M$ ($m^{-1}$/W) | $w_p$ (μm) | Cavity | $w_l$ (μm) | $I_{in}$ (5 %OC, MW/$cm^2$) | $I_{in}$ (10 %OC, MW/$cm^2$) |
|---|---|---|---|---|---|---|
| Yb:KLuW | 2.1 | 100 | Plano-concave | 42 ± 5 | 1.6 | 2.0 |
| | | | Plano-plano | 61 ± 5 | – | 0.6 |
| Yb:$LuVO_4$ | 3.7 | 100 | Plano-concave | 38 ± 5 | 5.2 | 2.5 |
| | | | Plano-plano | 44 ± 5 | 7.0 | 2.5 |

lens, both flat and concave OCs provide similar size of the laser mode (that is rather small) and, consequently, similar intracavity intensity values, about ~2.5 and 5–7 MW/$cm^2$ for 10 and 5 % OC, respectively. Both these values are much higher than the saturation intensity, so almost complete bleaching of the graphene-SA for the Yb:$LuVO_4$ laser is expected. It also explains the generation of shorter pulses with higher energies for this laser.

To model the characteristics of our graphene Q-switched lasers, we have solved the system of rate equations for a quasi-three-level laser material and fast saturable absorber:

$$\frac{dI_l}{dt} = \frac{c\mu}{n}[k_l - k_L - \frac{1}{l_a}\alpha_{SA}(I_l)]I_l + I_{noise}, \quad (1a)$$

$$\frac{dN_2}{dt} = \frac{I_p}{h\nu_p}k_p - \frac{I_l}{h\nu_l}k_l - \frac{N_2}{\tau}. \quad (1b)$$

Here, we have introduced two variables: (1) $I_l$—radiation intensity in the laser crystal at the laser frequency $\nu_l$ and (2) $N_2$—population of the upper laser level ($N_1 + N_2 = N_{Yb}$, where $N_1$ is the population of the ground-state and $N_{Yb}$ is the concentration of $Yb^{3+}$ ions). Both of these variables are considered as averaged over the crystal length and over the transverse dimensions. The remaining parameters are as follows: $c$ is the light velocity; $\mu = l_a n/l_c$ is the resonator filling factor; $l_a$ is the active element length; $n$ is the refractive index of the active element; $l_c$ is the optical length of the resonator, $k_l = N_2\sigma_l - N_{Yb}\sigma^l_{abs}$ is the gain coefficient at the laser frequency $\nu_l$ ($\sigma_l = \sigma^l_{SE} + \sigma^l_{abs}$, $\sigma^l_{SE}$ and $\sigma^l_{abs}$ are the stimulated-emission (SE) and absorption cross sections of the active material at the laser frequency $\nu_l$, respectively), $k_L = -[\ln(1 - T_{OC}) + \ln(1 - L)]/(2l_a)$ is the resonator loss coefficient, where $T_{OC}$ is the transmission of the output coupler and $L$ is the round-trip passive intracavity loss, $\alpha_{SA}$ is the loss coefficient in the saturable absorber, $I_{noise}$ is the noise rate, $I_p = I^p_{inc}[(1 - \exp(-k_p l_a))/k_p l_a]$ is the average pump intensity ($I^p_{inc} = P_{inc}/\pi w_p^2$ is the incident pump intensity, $P_{inc}$ is the incident pump power and $w_p$ is the pump spot radius), $h$ is the Planck constant, $\nu_p$ is the pump frequency, $k_p = N_{Yb}\sigma^p_{abs} - N_2\sigma_p$ is the absorption coefficient for the pump radiation ($\sigma_p = \sigma^p_{SE} + \sigma^p_{abs}$, $\sigma^p_{SE}$ and $\sigma^p_{abs}$ are the SE and absorption cross sections of the active material at the pump frequency $\nu_p$, respectively), $\tau$ is the lifetime of the upper laser level ($^2F_{5/2}$ level of $Yb^{3+}$).

The saturable absorption of graphene is typically described as [15, 16]:

$$\alpha'_{SA}(I_l) = \alpha'_{NS} + \frac{\alpha'_S}{1 + (I_l/I_{sat})}, \quad (2)$$

where $\alpha_{NS}{}'$ and $\alpha_S{}'$ are the non-saturable and saturable absorption of graphene, respectively (where the absorption, $\alpha'$, and transmission, $T$, are related as $\alpha' = 1 - T$, and $\alpha_{NS}{}' + \alpha_S{}' = 1 - T_{SA}$, $T_{SA}$ is the initial transmission of the graphene-SA) and $I_{sat}$ is the saturation intensity for graphene-SA. As already mentioned, for our graphene sample, the initial absorption was 2.2 %. For the modeling, the saturation intensity of a single-layer graphene at ~1 μm was taken as 1.0 MW/$cm^2$ [16]. Typically for a single-layer graphene, $\alpha_S{}'$ is considered to be 1.5 % [16]. However, our calculations for the lasers studied here indicated that the saturable absorption of the used graphene sample is lower, ~0.2 %. This explains the relatively high insertion loss for the graphene related to high non-saturable absorption.

The solution of Eqs. (1a, 1b) yielded a time-dependent intracavity laser intensity $I_l(t)$ which was used to calculate the output laser power, $P_{out}(t) = I_l(t)V_l k_{act}$, where $V_l = l_a\pi w_l^2/2$ is the volume of the laser mode in the active element ($w_l$ is the radius of the laser mode) and $k_{act}$ is the coefficient of the saturable losses, $k_{act} = -[\ln(1 - T_{OC})]/(2l_a)$. From the time-dependent $P_{out}(t)$, we have calculated the pulse duration (as FWHM), the pulse energy and the PRF for the Q-switched pulses. The material parameters of Yb:KLuW and Yb:$LuVO_4$ (absorption and SE cross sections, refractive indices and $^2F_{5/2}$ lifetime) used for the modeling are listed in Table 4. The results from the calculations are shown as solid curves in Figs. 4 and 6. The used model provides rather good agreement with the experimental data. The largest deviation of the calculated data from the experimental ones is observed for PRF which is lower than expected from modeling. However, the latter correctly represents the pulse energies. Thus, the modeling predicts the generation of higher average output power ($P_{out}$ = PRF·$E_{out}$) than observed in the experiment. We refer this to the temperature variation of the spectroscopic properties of the laser crystal which can lead to the drop in laser output.

The developed Yb:KLuW and Yb:$LuVO_4$ lasers with a plano-plano cavity represent the first step to Yb microchip

**Table 4** Material properties of Yb:KLuW and Yb:$LuVO_4$ used for modeling of the Q-switched laser performance, in accordance with [1, 10]

| Parameter | Notation | Unit | Yb:KLuW ($E\|\|N_m$) | Yb:$LuVO_4$ ($E\|\|c$) |
|---|---|---|---|---|
| Absorption cross section | $\sigma^p_{abs}/\sigma^l_{abs}$ | $10^{-20}$ cm$^2$ | 3.0/0.2 | 3.1/0.2 |
| SE cross section | $\sigma^l_{SE}/\sigma^p_{SE}$ | $10^{-20}$ cm$^2$ | 2.3/3.2 | 1.4/3.0 |
| Refractive index | $n$ | | 2.0294 | 2.249 |
| Lifetime of the $^2F_{5/2}$ state | $\tau$ | μs | 275 | 256 |

Superscripts "p" and "l" correspond to the values at the pump and laser wavelengths, respectively

**Table 5** Comparison of the output characteristics of the current Yb lasers passively Q-switched with graphene-SA

| Laser/type | $P_{out}$ (mW) | $\eta$ (%) | $\tau$ (ns) | PRF (kHz) | $E_{out}$ (μJ) | Refs. |
|---|---|---|---|---|---|---|
| Yb:$KY(WO_4)_2$/waveguide | 34 | 9 | 349 | 607 | 0.059 | [19] |
| Yb:$Y_2O_3$/waveguide | 83 | 25 | 98 | 1040 | 0.080 | [20] |
| Yb:$Y_2O_3$/waveguide | 456 | 13 | 158 | 1470 | 0.33 | [30] |
| Yb:glass/waveguide | 21 | 3 | 140 | 833 | 0.027 | [18] |
| Yb/fiber | 12 | – | 70 | 257 | 0.046 | [21] |
| Yb/fiber | 16 | – | 1300 | 110 | 0.142 | [22] |
| Yb/fiber | 35 | – | 1600 | 55 | 0.65 | [23] |
| Yb:$KLu(WO_4)_2$/bulk | 170 | 12 | 165 | 350 | 0.49 | This work |
| Yb:$LuVO_4$/bulk | 300 | 10 | 152 | 360 | 0.83 | This work |
| Yb:YAG/bulk | 185 | 12 | 228 | 285 | 0.65 | [29] |

lasers passively Q-switched with graphene. For these lasers, the stabilization of the laser mode is provided by the positive thermal lens ($M > 0$). Although positive sign of the thermal lens is inherent for tetragonal vanadates due to the positive thermo-optical coefficients ($dn/dT$) [5], the positive thermal lens for Yb:KLuW (with $dn/dT < 0$) is provided by the special crystal cut along the $N_g$-axis. For this crystal cut, positive impact of thermal expansion of the laser element compensates negative impact of $dn/dT$ [28]. It should be noted that in our previous work on graphene PQS of Yb:YAG [29], the attempt to build a Q-switched microchip laser failed mainly due to the weak positive thermal lens in this crystal, with $M \sim 1.7$ m$^{-1}$/W, and hence, the weak mode confinement in the cavity was not enough to bleach the graphene-SA, and thus, a curved output coupler had to be used.

In Table 5, we compare the performance of graphene-SA Q-switched Yb lasers developed previously and in the present work. With a Yb:$Y_2O_3$ waveguide laser, sub-100 ns pulses were achieved, however, with a much lower pulse energy (0.08 μJ) [20] than in the present work. Later on in [30], this result was improved, generating 158 ns/0.33 μJ pulses. Low pulse energies were due to a very high PRF reaching the MHz level. Yb fiber lasers permit optimization of either pulse duration or energy but not both, so the achieved parameters, 70 ns/0.046 μJ [21] or 1600 ns/0.65 μJ [23], are not comparable with our results with bulk lasers in terms of peak power.

Further optimization of graphene-SA Q-switched compact Yb lasers is possible with the use of multilayered graphene ($n = 2\ldots4$) that can provide an increased modulation depth and, hence, shorten the pulses to ~10 ns with pulse energy reaching >10 μJ, as it can be expected from the modeling. In particular, the compactness of the laser cavity is clearly beneficial when using graphene because it allows for a reduction in the pulse duration with respect to the standard hemispherical cavities by a factor of ~10, as recently shown for graphene-SA Q-switched Tm:KLuW microchip laser [25]. The microchip lasers also offer the possibility of direct deposition of graphene on the crystal face without the need of additional focusing. An important question for power scaling is then the reduction in the unwanted heating of the SA by the residual pump that is inherent to the microchip design. This can be done by increasing the Yb doping concentration which is possible for the KLuW crystal.

Improvement in the quality of the graphene-SA is essential for minimization of its insertion loss and, thus, to increase the laser slope efficiency. In our experiments, both laser crystals were uncoated. This did not affect the Q-switched laser performance (it just contributed to the passive intracavity losses). However, AR coatings on crystal surfaces will potentially improve the laser efficiency.

## 4 Conclusions

We report on bulk Yb lasers passively Q-switched with a single-layer graphene-SA. It is shown that although graphene possesses a high saturation intensity at ~1 μm, it can

be used to provide stable PQS of Yb lasers when using a compact laser setup (including the microchip-like configuration), as well as active materials with a strong thermal lens. These are the factors that can provide deep bleaching of the SA due to a strong mode confinement, and generation of nanosecond pulses both due to the reduction in the cavity roundtrip time and to the above-mentioned deep bleaching. With the compact (~4-mm-long), diode-pumped Yb:KLuW and Yb:$LuVO_4$ lasers, we achieved 165 ns/0.49 μJ and 152 ns/0.83 μJ pulses, respectively. The maximum average output power from the Yb:$LuVO_4$ laser with the plano-plano cavity reached 310 mW at 1021 nm with 17 % slope efficiency (corresponding to 240 ns pulses and a PRF of 330 kHz). Further improvement in the output characteristics of graphene Q-switched Yb lasers is expected with the use of multilayered graphene.

**Acknowledgments** This work was supported by the Spanish Government under projects MAT2013-47395-C4-4-R and TEC2014-55948-R, and by the Generalitat de Catalunya under Project 2014SGR1358. F.D. acknowledges additional support through the ICREA Academia Award 2010ICREA-02 for excellence in research. This work is part of a project that has received funding from the European Union's Horizon 2020 research and innovation programme under the Marie Skłodowska-Curie Grant Agreement No. 657630.

## References

1. V. Petrov, M.C. Pujol, X. Mateos, O. Silvestre, S. Rivier, M. Aguiló, R.M. Solé, J. Liu, U. Griebner, F. Díaz, Laser Photonics Rev. **1**, 179 (2007)
2. V.E. Kisel, A.E. Troshin, N.A. Tolstik, V.G. Shcherbitsky, N.V. Kuleshov, V.N. Matrosov, T.A. Matrosova, M.I. Kupchenko, Opt. Lett. **29**, 2491 (2004)
3. J. Petit, B. Viana, P. Goldner, D. Vivien, P. Louiseau, B. Ferrand, Opt. Lett. **29**, 833 (2004)
4. Y. Sato, T. Taira, Opt. Express **14**, 10528 (2006)
5. P.A. Loiko, K.V. Yumashev, V.N. Matrosov, N.V. Kuleshov, Appl. Opt. **52**, 698 (2013). **[Erratum: Appl. Opt. 54, 4820 (2015)]**
6. M.C. Pujol, M.A. Bursukova, F. Guell, X. Mateos, R. Solé, Jna. Gavaldà, M. Aguiló, J. Massons, F. Díaz, P. Klopp, U. Griebner, V. Petrov, Phys. Rev. B **65**, 165121 (2002)
7. J.M. Serres, P. Loiko, X. Mateos, K. Yumashev, N. Kuleshov, V. Petrov, U. Griebner, M. Aguiló, F. Díaz, Opt. Mater. Express **5**, 661 (2015)
8. S. Rivier, X. Mateos, Ò. Silvestre, V. Petrov, U. Griebner, M.C. Pujol, M. Aguiló, F. Díaz, S. Vernay, D. Rytz, Opt. Lett. **33**, 735 (2008)
9. J. Liu, V. Petrov, X. Mateos, H. Zhang, J. Wang, Opt. Lett. **32**, 2016 (2007)
10. J. Liu, V. Petrov, H. Zhang, J. Wang, M. Jiang, Opt. Lett. **31**, 3294 (2006)
11. J. Liu, V. Petrov, H. Zhang, J. Wang, Appl. Phys. B **88**, 527 (2007)
12. S. Rivier, X. Mateos, J. Liu, V. Petrov, U. Griebner, M. Zorn, M. Weyers, H. Zhang, J. Wang, M. Jiang, Opt. Lett. **14**, 11668 (2006)
13. U. Griebner, S. Rivier, V. Petrov, M. Zorn, G. Erbert, M. Weyers, X. Mateos, M. Aguiló, J. Massons, F. Díaz, Opt. Express **13**, 3465 (2005)
14. R.R. Nair, P. Blake, A.N. Grigorenko, K.S. Novoselov, T.J. Booth, T. Stauber, N.M.R. Peres, A.K. Geim, Science **320**, 1308 (2008)
15. Q.L. Bao, H. Zhang, Y. Wang, Z. Ni, Y. Yan, Z.X. Shen, K.P. Loh, D.Y. Tang, Adv. Funct. Mater. **19**, 3077 (2009)
16. F. Zhang, S. Han, Y. Liu, Z. Wang, X. Xu, Appl. Phys. Lett. **106**, 091102 (2015)
17. G. Xing, H. Guo, X. Zhang, T.C. Sum, C.H.A. Huan, Opt. Express **18**, 4184 (2010)
18. A. Choudhary, S. Dhingra, B. D'Urso, P. Kannan, D.P. Shepherd, IEEE Photonics Technol. Lett. **27**, 646 (2015)
19. J.W. Kim, S.Y. Choi, S. Aravazhi, M. Pollnau, U. Griebner, V. Petrov, S. Bae, K.J. Ahn, D.-I. Yeom, F. Rotermund, AIP Adv. **5**, 017110 (2015)
20. A. Choudhary, S. Dhingra, B. D'Urso, T.L. Parsonage, K.A. Sloyan, R.W. Eason, D.P. Shepherd, Opt. Lett. **39**, 4325 (2014)
21. J. Liu, S. Wu, Q.-H. Yang, P. Wang, Opt. Lett. **36**, 4008 (2011)
22. L. Zhang, J.T. Fan, J.H. Wang, J.M. Hu, M. Lotya, G.Z. Wang, R.H. Li, L. Zhang, W.J. Blau, J.N. Coleman, J. Wang, Y. Feng, Laser Phys. Lett. **9**, 888 (2012)
23. L. Zhang, Z. Zhuo, R. Wei, Y. Wang, X. Chen, X. Xu. Chin. Opt. Lett. **12**, 021405 (2014)
24. A.C. Ferrari, J.C. Meyer, V. Scardaci, C. Casiraghi, M. Lazzeri, F. Mauri, S. Piscanec, D. Jiang, K.S. Novoselov, S. Roth, A.K. Geim, Phys. Rev. Lett. **97**, 187401 (2006)
25. J.M. Serres, P. Loiko, X. Mateos, K. Yumashev, U. Griebner, V. Petrov, M. Aguiló, F. Díaz, Opt. Express **23**, 14108 (2015)
26. D. Yoon, Y.W. Son, H. Cheong, Nano Lett. **11**, 3227 (2011)
27. P. Loiko, F. Druon, P. Georges, B. Viana, K. Yumashev, Opt. Mater. Express **4**, 2241 (2014)
28. P.A. Loiko, J.M. Serres, X. Mateos, K.V. Yumashev, N.V. Kuleshov, V. Petrov, U. Griebner, M. Aguiló, F. Díaz, Laser Phys. Lett. **11**, 125802 (2014)
29. J.M. Serres, V. Jambunathan, X. Mateos, P. Loiko, A. Lucianetti, T. Mocek, K. Yumashev, V. Petrov, U. Griebner, M. Aguiló, F. Díaz, IEEE Photonics J. **7**, 1503307 (2015)
30. A. Choudhary, S.J. Beecher, S. Dhingra, B. D'Urso, T.L. Parsonage, J.A. Grant-Jacob, P. Hua, J.I. Mackenzie, R.W. Eason, D.P. Shepherd, Opt. Lett. **40**, 1912 (2015)